15

Antenna measurements

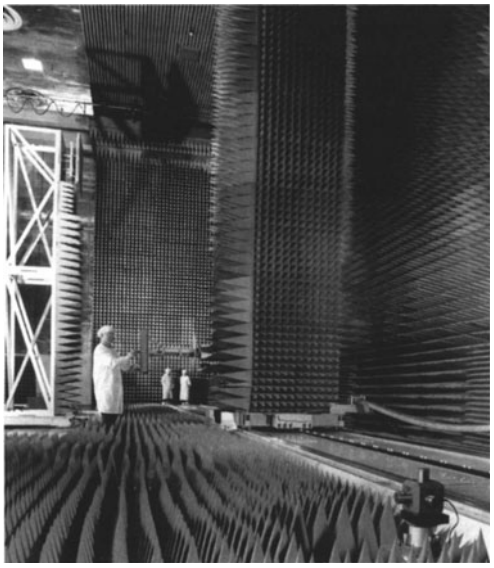

Planar near-field scanner at EADS Astrium, Portsmouth, England. This is used to measure antennas on remote sensing and communications satellites, and has a scan area of 22 m x 8 m. It is believed to be the largest such facility in the world. (photo: EADS Astrium)

15.1 INTRODUCTION

Antenna measurements are important both to the antenna designer and the antenna manufacturer. Measurement is an integral part of the design process, and the results of measurement of a prototype may be fed back to iteratively refine the design. In manufacture, it will be necessary to check that the performance of a product meets certain specifications.

There are a wide range of antenna parameters that can be measured. The key ones are the gain and the radiation pattern, but input impedance (and hence bandwidth) can also be important. For the radiation pattern, usually a 1-D cut as a function of azimuth angle, at a single polarization, is adequate, though the full 2-D co-polar and

cross-polar patterns may be required for some applications. The purpose of this chapter is therefore to describe the principles of the various measurement techniques that are used and explain their advantages and disadvantages. A brief and selective description of some current research topics is also given in each case.

15.2 GAIN MEASUREMENTS

15.2.1 Comparison with a standard-gain horn

The signal obtained from the antenna under test is compared by substitution with that from an antenna of known gain, such as a standard-gain horn, with constant power transmitted from the source antenna, under controlled conditions such as an anechoic chamber or test range. The gain G of the antenna under test is simply given by

$$G = P_R . \frac{G_S}{P_S} \tag{15.1}$$

where P_R is the power accepted by the antenna under test, G_S is the gain of the standard-gain horn and P_S is the power accepted by the standard gain horn, allowing for any mismatches. The advantage of this method is that it does not rely on knowledge of the path loss due to the distance between the source antenna and the antenna under test.

15.2.2 Two-antenna measurement

The Friis transmission equation (see §4.2.1) establishes the power received by the antenna under test as

$$P_R = \frac{P_S G_S G \lambda^2}{(4\pi)^2 r^2} \tag{15.2}$$

So if P_S, G_S, λ and r are known, a measurement of P_R allows G to be determined. If G_S is not known, then identical test antennas may be used at both the transmit and receive ends of the path to establish their gain.

Alternatively, the return signal from a single test antenna facing a large conducting sheet may be used to measure its gain (the effective chamber length being twice the separation of the antenna and the sheet). This is known as *Purcell's method*. It is important that the inherent mismatch of the test antenna is taken into account.

15.2.3 Three-antenna measurement

If three antennas of unknown gains G_1, G_2 and G_3 are used as source and test antennas in all three possible combinations, denoting the source power by P_S, the received powers are

$$P_{12} = \frac{P_S G_1 G_2 \lambda^2}{(4\pi)^2 r^2} \qquad P_{23} = \frac{P_S G_2 G_3 \lambda^2}{(4\pi)^2 r^2} \qquad P_{13} = \frac{P_S G_1 G_3 \lambda^2}{(4\pi)^2 r^2} \tag{15.3}$$

These can be solved for G_1, G_2 and G_3, giving

$$\boxed{G_1 = \frac{4\pi r}{\lambda}\sqrt{\frac{P_{13}P_{12}}{P_S P_{23}}} \qquad G_2 = \frac{4\pi r}{\lambda}\sqrt{\frac{P_{23}P_{12}}{P_S P_{13}}} \qquad G_3 = \frac{4\pi r}{\lambda}\sqrt{\frac{P_{13}P_{23}}{P_S P_{12}}}} \tag{15.4}$$

This method, again, does not rely on the use of a standard gain antenna, but does require knowledge of the path length between the source and test ends of the chamber, and of the source power P_S.

15.2.4 Extrapolation

The most accurate method currently in use is that developed by Newell *et al.*[1] at the National Institute of Standards and Technology (NIST) in the USA, and refined by workers at the National Physical Laboratory (NPL), Teddington, UK. These laboratories (amongst others) provide a calibration service for antenna gains.

The method is a development of the three-antenna technique, but eliminates the uncertainty in knowledge of the path loss. This may arise because of difficulties in locating the exact phase centre of each antenna (is it at the aperture of a horn or at its 'throat' ?). To overcome this, measurements are made at a number of separations of source and test antennas and a polynomial fitted to the measurements using a least-squares technique, and then extrapolated to infinite range. In the NPL method, the polynomial also includes sine and cosine terms to model the oscillations due to multiple reflections.

If the measurements are to be made at a number of frequencies over a band (as would usually be the case), then the procedure has to be automated under computer control. An overall accuracy of better than ±0.04 dB is claimed. Fig. 15.1 shows this technique being used for the measurement of the gain of a log spiral antenna.

---

[1] Newell, A.C., Baird, R.C. and Wacker, P.F., 'Accurate measurement of antenna gain and polarisation at reduced distances by an extrapolation technique', *IEEE Trans. Antennas & Propagation*, Vol. AP-21, No. 4, April 1973.

Fig. 15.1 Gain calibration of a log-spiral antenna, being carried out in an anechoic chamber at the National Physical Laboratory, Teddington, UK (Crown copyright).

15.3 RADIATION PATTERN MEASUREMENTS

Measurements of radiation pattern and of gain are best performed in an unobstructed medium without the presence of any objects that might give rise to reflections. Either a large outdoor test range or (more commonly) an anechoic chamber may be used. Outdoor test ranges allow a greater distance between the source antenna and the antenna under test (and hence a better approximation to a plane wave), but may be undesirable if one does not want to reveal the antenna under test for reasons of commercial or military security. Fig. 15.2 shows an example of a typical outdoor test range.

Fig. 15.2 The outdoor test range at Funtington in Southern England (Crown copyright).

15.3.1 Anechoic chambers and far-field ranges

An anechoic chamber (Fig. 15.3) consists of an enclosed room with a source antenna at one end which is used to excite the antenna under test at the other end. The antenna under test is mounted on a turntable or multi-axis positioner which is rotated to obtain its radiation pattern. The chamber is lined with Radio Absorbing Material (RAM) which minimizes reflections from the walls, floor and ceiling. Chambers are sometimes tapered to prevent the formation of standing waves.

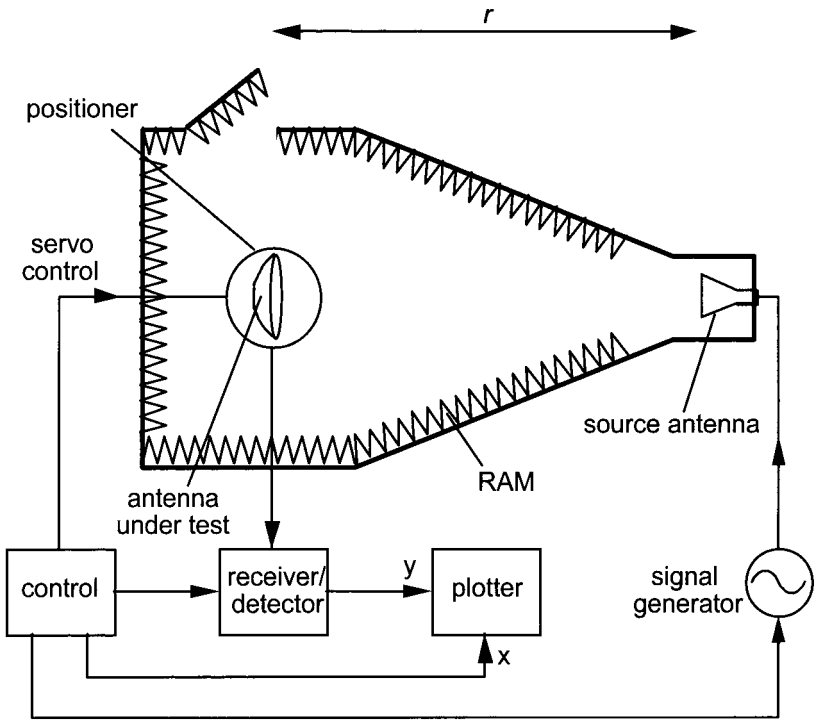

Fig. 15.3 Features of a typical anechoic chamber and its instrumentation.

RAM [1] is made from carbon-impregnated polyurethane foam (or similar), and usually has a tapered pyramidal shape, which in effect provides a gradual transition between the impedance of free space and that of the metal sheet that forms the walls of the chamber. Figure 15.4 shows typical RAM of this kind. Reflection coefficients of typically –20 to –40 dB are obtainable over a range of incidence angles and frequencies, for absorber thicknesses of the order of a few wavelengths. More sophisticated absorbers can be made from multi-layer structures, but these are only used in specialized applications.

As well as being rotatable in azimuth, the antenna under test may be tilted in elevation. Also, the source antenna may be rotated about its axis for polarization measurements (see §15.2.6). The chamber is usually arranged to transmit from the source antenna and receive on the antenna under test, although this arrangement may be reversed if it is more convenient. The turntable positioner, plotter, receiver and transmit source are usually all under computer control, and purpose-built suites of instrumentation are available from manufacturers such as Orbit, Agilent and Scientific Atlanta.

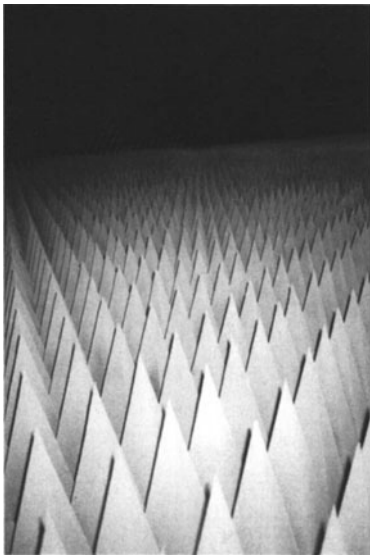

Fig. 15.4 Typical pyramidal RAM in an anechoic chamber (photo: H. Griffiths).

These types of antenna measurements are performed in the far field - that is to say, the antenna under test is illuminated by a plane wave. To obtain a perfect plane wave the range would have to be infinitely long, but for practical purposes it is usual to adopt a criterion such that the phase error at the edge of the curved wavefront should not exceed $\pi/8$ radians (22.5°).

From Fig. 15.5 it can be seen that the spherical wavefront from the source antenna gives rise to a path difference at the edge of the antenna under test of

$$\Delta x = \left(r^2 + D^2/4\right)^{1/2} - r$$

The bracket can be expanded, and taking just the first two terms of the expansion

$$\Delta x = \left(r + \frac{D^2}{8r} + \ \ldots\right) - r \tag{15.5}$$

which corresponds to a phase difference of

$$\Delta\phi = \frac{2\pi}{\lambda}.\Delta x = \frac{\pi D^2}{4r\lambda}$$

Setting this = $\pi/8$ gives

$$r = \frac{2D^2}{\lambda} \tag{15.6}$$

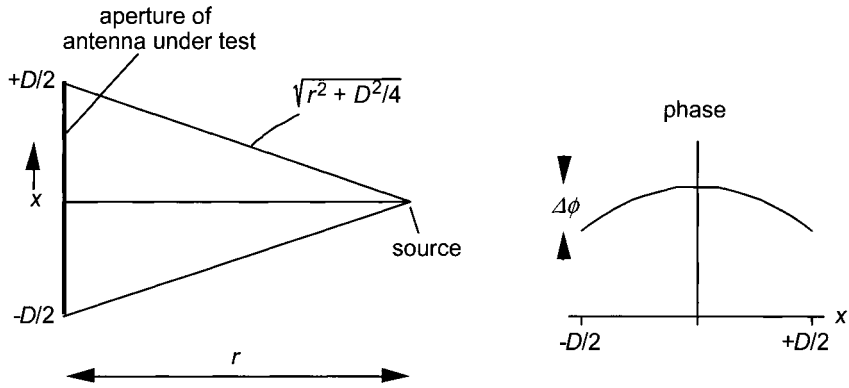

Fig. 15.5 Derivation of the Rayleigh distance criterion.

This is known as the *Rayleigh distance*. In practice one would like to arrange that the distance between the source antenna and the antenna under test is at least one Rayleigh distance, and preferably more. Clearly this constraint becomes more of a problem the larger the antenna under test, and the higher the frequency.

There are two other minimum chamber length criteria which may need to be considered, particularly at low frequencies. Firstly, the reactive near field will be significant within about one wavelength of the antenna, so we require that $r > \lambda$. Secondly, when the antenna is rotated, the distance from one end to the source varies from $r + D/2$ to $r - D/2$. The $1/r$ field dependence can give rise to pattern errors. If, for example, ±0.5 dB amplitude error is acceptable, then $r > 10D$ is required.

The volume within which the phase and amplitude errors of the wavefront are sufficiently low is known as the *quiet zone*. A criterion such that the errors should be less than ±0.5 dB (amplitude) and ±5° (phase) is usual (this question is considered further in §15.2.3).

At low frequencies (< 1 GHz, say) an open test range would normally be used. This is because any chamber would need to be very long to operate in the far field, and also a large volume of RAM would be needed, since the RAM depth needs to be two wavelengths or more to minimize the reflectivity.

The usable dynamic range of an antenna range is limited by two main factors:

(1) The source transmit power and receiver sensitivity. This is not a serious limitation provided that the signal is detected in a narrow bandwidth and a wide dynamic range low-noise amplifier is used at the test antenna.

(2) The finite reflectivity of the chamber walls, or other objects within the chamber. These reflections degrade the quality of the plane wave with which the antenna under test is illuminated. Multiple reflections 'fill in' nulls in the radiation pattern and create 'phantom' sidelobes. Naturally, these effects will be most troublesome in the measurement of low-sidelobe antennas. This question is considered further in §15.2.3.

The peak power received by the antenna under test (when it is pointing directly at the source antenna) is given by equation (15.2). If the required dynamic range of the measurement is X dB, then the minimum detectable signal must be at least X dB below this figure, and preferably slightly more if measurements of nulls between sidelobes are not to be corrupted by noise.

15.3.2 Compact ranges

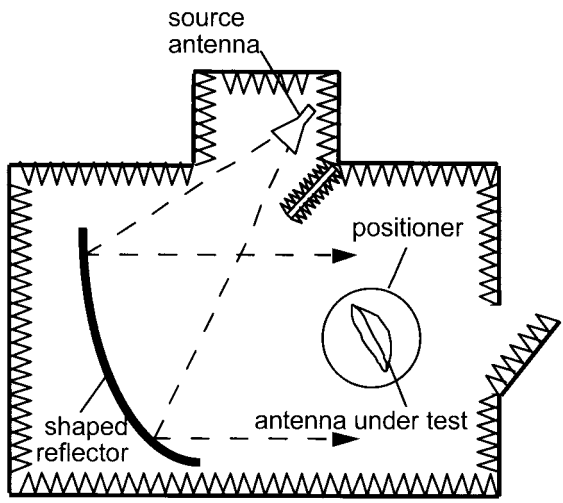

Fig. 15.6 A single-offset-fed compact antenna test range (CATR).

Evidently, for large antennas and high frequencies the amount of 'real estate' needed to get far enough away to achieve a good approximation to a plane wave can become prohibitive, and this has caused engineers to consider other techniques. Chief among

these is the *compact range*, or *compact antenna test range* (CATR), originated by R.C. Johnson[2] at Georgia Tech, where much of the innovative work on antenna measurements has been done during the past few decades. The compact range uses an offset-fed parabolic reflector to synthesize a plane wave in a considerably more compact configuration than that of a conventional range. The reflectors and their feeds are designed using the techniques established in §10.3.

Fig. 15.6 shows the typical features of a compact range. Note the shielding between the source antenna and the turntable, to minimize leakage of the direct signal. The key component in a compact range is the reflector, and this is designed in exactly the same way as for an offset-fed reflector antenna. It is usually constructed from a set of shaped panels, whose positions are individually set up during alignment (often using laser-ranging techniques) by means of lead screws. To minimize diffraction from the edges of the reflector, the edges may either be serrated or rolled.

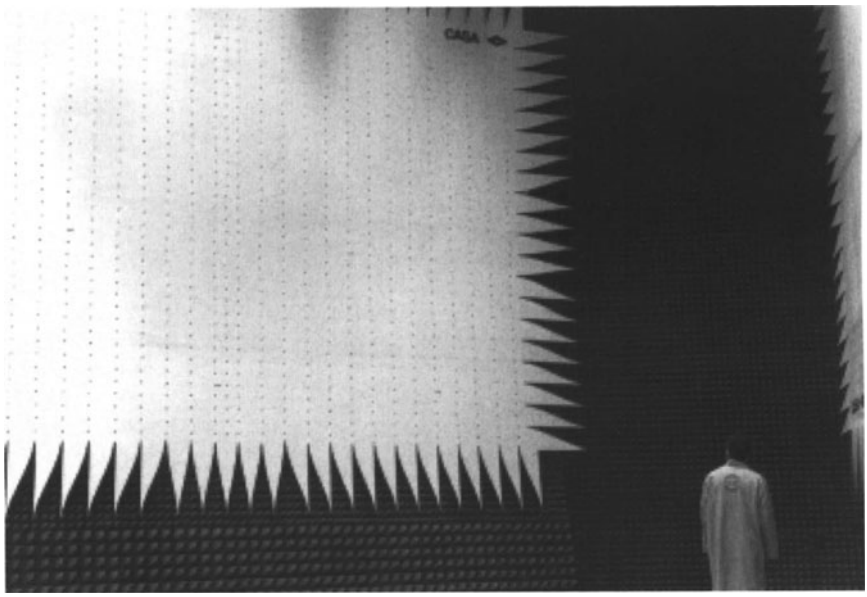

Fig. 15.7 The enormous compact range at the European Space Agency's ESTEC facility at Noordwijk in the Netherlands. This is used for pre-launch testing of antennas on satellites, so the positioner has to be large enough to accommodate complete satellites. The range uses a dual-reflector configuration to give high polarization purity for measurements on dual-polarized antennas. Note also the serrated edges of the reflectors. (photo: H. Griffiths).

[2] Johnson, R.C., 'Antenna range for providing a plane wave for antenna measurements', US patent 3302205, 31 January 1967.

In a variant of the scheme two reflectors are used in a reflex configuration. This gives better control over generation of cross-polarization, so the dual-reflector compact range is often preferred for measurements on antennas where high cross-polar performance is important, such as satellite communications antennas. Two interesting examples of compact ranges are shown in Figs. 15.7 and 15.8.

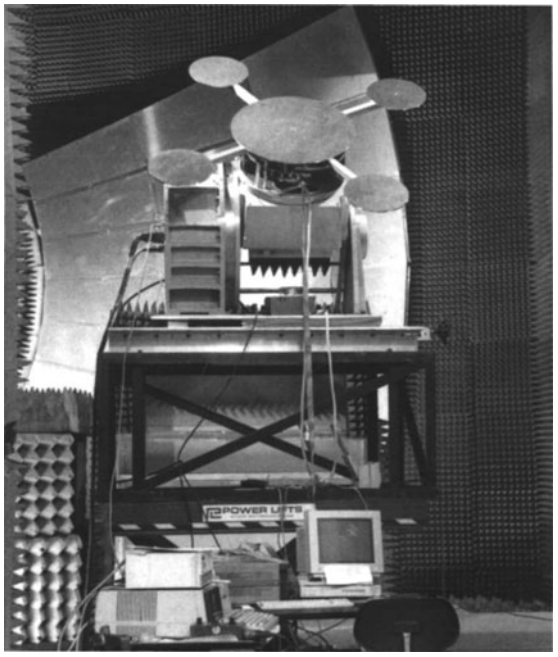

Fig. 15.8 The mm-wave compact range at Queen Mary College, University of London. This is capable of working up to 200 GHz. The reflector is a single offset antenna of 5.4 m focal length, made up of 18 panels, with an rms accuracy of approximately 60 microns. The quiet zone is 1 m × 1 m × 1 m. The antenna under test is a symmetric-pair array developed for direction-finding applications (§11.8.6). (photo: Dr W. Titze).

15.3.3 Wavefront quality

We have already remarked that the accuracy of radiation pattern measurements depends on the quality of the plane wave with which the antenna is illuminated, and both the finite distance of the source antenna and reflections from the walls of the anechoic chamber will cause the illumination to depart from a perfect plane wave.

These effects can be quantified in terms of plane wave spectra[3] [4], as introduced in §2.1.

A perfect plane wave travelling normal to the aperture corresponds to uniform phase and uniform amplitude over that aperture. If we assume for the moment that this aperture is infinite in extent, then the plane wave spectrum is just a single Dirac delta function at the origin. On the other hand, a plane wave incident from a different direction will give uniform amplitude, but phase varying linearly with direction over the aperture, and the plane wave spectrum will be a delta function whose position corresponds to the direction of incidence.

By taking a set of samples over a plane in the quiet zone and computing the 2-D Fourier Transform, we can therefore determine the directions and levels of the wavefront components. Clearly, if we want to measure sidelobe levels (for example) < -40 dB, we need to be sure that no other component of the plane wave spectrum exceeds this level. A more recent idea is that if the plane wave spectrum of the illumination can be measured, it should in principle be possible to deconvolve it from the measurement of the antenna radiation pattern, and hence remove the effects of imperfections in the illumination.

15.3.4 Near-field techniques

An alternative to illuminating the antenna under test with a plane wave, and rotating it to obtain one cut of the radiation pattern, is to transmit a signal from the antenna under test and sample the radiated signal (in both amplitude and phase) in the near field. From a knowledge of the near-field signal, the far-field radiation pattern can be computed. This permits a very compact measurement system, and the whole 3-D radiation pattern can be derived rather than just one cut; however, the full sampling of a large aperture may take some time, and also the probe antenna must be positioned very accurately. Furthermore, the flexible cable that connects the probe to the measurement receiver must have very stable phase characteristics, and it is necessary to ensure that the probe does not itself perturb the field that it is trying to measure.

There are three geometries that are used. In *planar near-field scanning* the antenna under test is fixed and the probe is scanned over the antenna aperture plane by means of an *x-y* positioner. In *cylindrical near-field scanning* the probe is scanned vertically, while the antenna under test is rotated. The calculation of the far-field pattern is carried out in cylindrical polar co-ordinates. The cylindrical geometry

---

[3] Booker, H.G. and Clemmow, P.C., 'The concept of an angular distribution of plane waves and its relation to that of a polar diagram and aperture distribution', *JIEE*, Vol. 97, 1950, pp11-17.

[4] Bennett, J.C. and Farhat, K.S., 'Waveform quality in antenna pattern measurement: the use of residuals', *Proc. IEE*, Vol. 134, Pt. H, No. 1, pp30-34, February 1987.

avoids the complication of an *x-y* positioner, since the probe is only scanned in one dimension, though a turntable is required to rotate the antenna under test, as well as a phase-stable rotating joint. In *spherical near-field scanning* the probe is scanned over a spherical surface (or the probe held fixed and the antenna under test rotated).

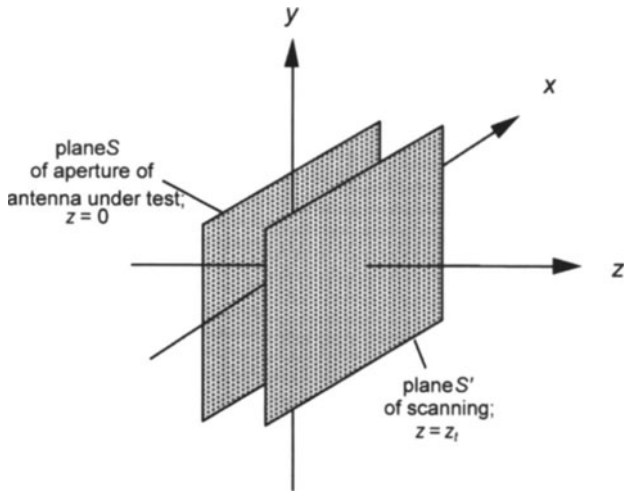

Fig. 15.9 Geometry of planar near-field scanning.

Planar scanning is probably the most frequently-used, because most antennas of practical interest are directive, and have a well-defined planar region over which to make the measurement. Following the treatment of Wang [4], and noting also the results on plane wave spectra obtained in §2.1, suppose that the antenna aperture lies in plane S defined by the xy plane at $z = 0$. The field is sampled in the plane S', at $z = z_t$ (Fig. 15.9). The plane wave spectrum $\mathbf{A}(k_x, k_y)$ of the radiation is related to the field $\mathbf{E}(x, y, z_t)$ sampled at S' by

$$E_x(x, y, z_t) = \frac{1}{2\pi} \int_{-\infty}^{\infty} \int_{-\infty}^{\infty} A_x(k_x, k_y) . \exp(-jk_z z_t) \exp\left[-j(k_x x + k_y y)\right] dk_x dk_y \tag{15.7}$$

$$E_y(x, y, z_t) = \frac{1}{2\pi} \int_{-\infty}^{\infty} \int_{-\infty}^{\infty} A_y(k_x, k_y) \exp(-jk_z z_t) \exp\left[-j(k_x x + k_y y)\right] dk_x dk_y \tag{15.8}$$

From these, the aperture field $\mathbf{E}(x,y,0)$ can be obtained

$$E_x(x,y,0)=\frac{1}{2\pi}\int_{-\infty}^{\infty}\int_{-\infty}^{\infty}A_x(k_x,k_y)\exp\left[-j(k_x x+k_y y)\right]dk_x dk_y \tag{15.9}$$

$$E_y(x,y,0)=\frac{1}{2\pi}\int_{-\infty}^{\infty}\int_{-\infty}^{\infty}A_y(k_x,k_y)\exp\left[-j(k_x x+k_y y)\right]dk_x dk_y \tag{15.10}$$

and hence the far-field radiation pattern, by Fourier transformation of $\mathbf{E}(x,y,0)$.

The required sample spacing in the plane S', according to the sampling theorem, should be no greater than $\lambda/2$. In practice a sample spacing of $\sim\lambda/3$ would be appropriate.

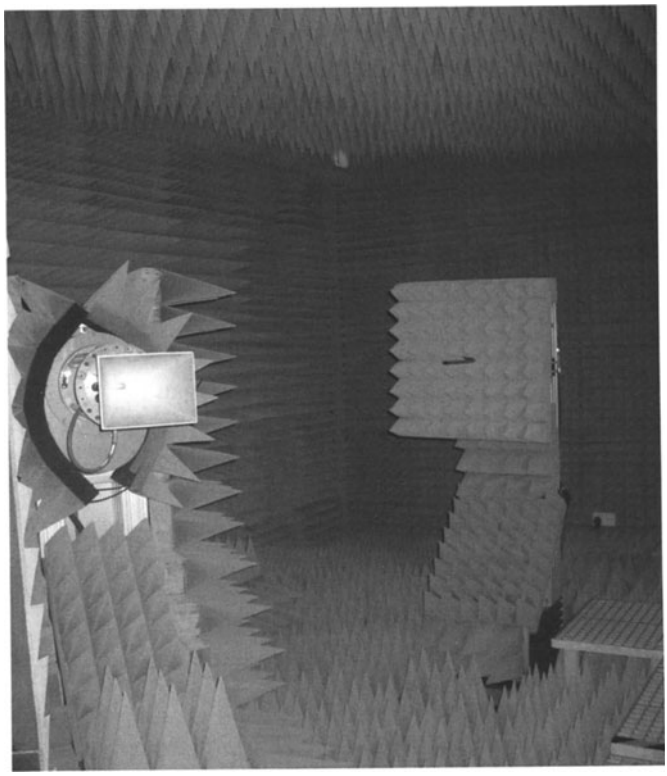

Fig. 15.10 Spherical near-field scanning system at University College London (installed by MI Technologies, Atlanta, USA, May 2005).

The simple theory assumes that the probe acts as a perfect point receiver. In practice this will not be the case, so the technique of *probe compensation*[5] was developed, characterizing and compensating for the angular response of the probe antenna.

Near-field techniques are therefore quite attractive, and a few years ago an entire Special Issue of *IEEE Transactions on Antennas and Propagation* was devoted to advances in the subject [8].

15.3.5 Other techniques

Rather than measuring the aperture field directly with a probe, it is also possible to scatter it in some way back into the antenna under test and measure the change in reflection coefficient at the antenna feedpoint due to the scattered signal. If the scattering is modulated, then the scattered signal can be distinguished from the static component of the reflection coefficient by synchronous detection. This technique was originally developed at University College London back in the 1950s by Cullen and Parr, using so-called 'spinning dipoles' to modulate the scattered field[6], and also independently by Richmond in the USA[7]. The technique has been used more recently by Bolomey and co-workers at *Supelec* near Paris and in their spin-out company *SATIMO*, using an array of dipoles modulated electronically by PIN diodes at their feedpoints. In one implementation[8] the antenna under test is rotated slowly through 360° while the dipoles are modulated sequentially (Fig. 15.11). The use of an array of modulated scatterers has advantages in respect of the time taken to complete the measurement. The scattered signal may be received either monostatically by the antenna under test, or bistatically by a second, fixed test antenna, which gives advantages in respect of dynamic range. This gives a rapid measurement of the full 3-D radiation pattern in a single scan.

---

[5] Kerns, D.M., 'Correction of near-field antenna measurements made with an arbitrary but known measuring antenna', *Electronics Letters*, Vol. 6, pp346-347, May 1970.

[6] Cullen, A.L. and Parr, J.C., 'A new perturbation technique for measuring microwave fields in free space', *Proc. IEE*, Vol. 102, Part B, No. 6, pp836-844, November 1955.

[7] Richmond, J.H., 'A modulated scattering technique for the measurement of field distributions', *IRE Trans. Microwave Theory and Techniques*, Vol.3, pp13-15, 1955.

[8] Bolomey, J-Ch. *et al.*, 'Rapid near-field antenna testing via arrays of modulated scattering probes', *IEEE Trans. Antennas & Propagation*, Vol. AP-36, No. 6, pp804-814, June 1988.

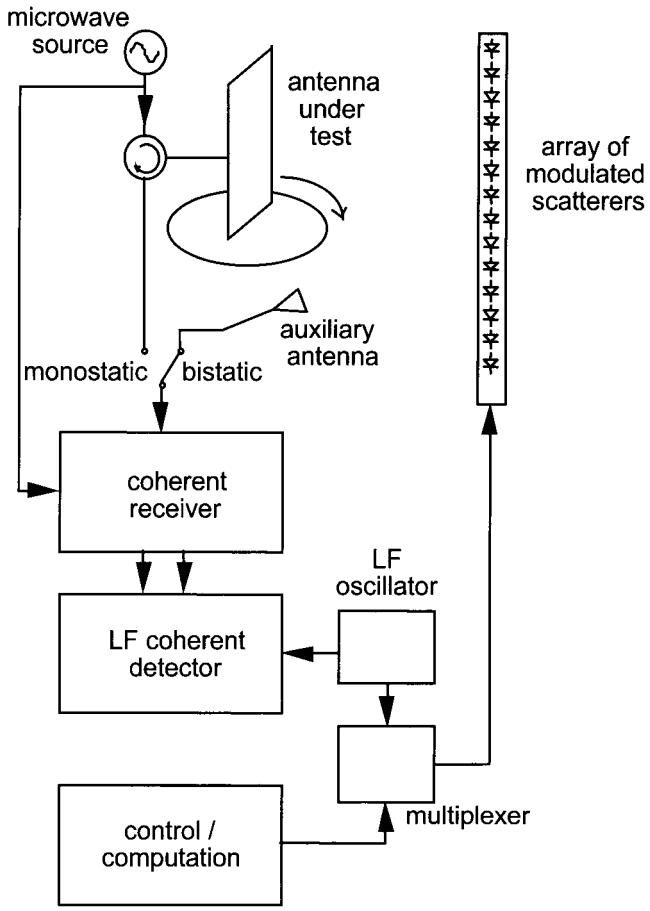

Fig. 15.11 Experimental arrangement of modulated scatterer radiation pattern measurement technique employed by Bolomey *et al.* (adapted from reference 8).

Another implementation of this type of technique uses the scattering from a wire, which is moved across the aperture of the antenna under test[9]. It can be shown that the change in reflection coefficient measured at the antenna feed is proportional to the square of the aperture field at the position of the wire, integrated along the wire.

---

[9] Calazans, E.T., Griffiths, H.D., Cullen, A.L., Davies, D.E.N. and Benjamin, R., 'Antenna radiation pattern measurement using a near-field wire scattering technique'; *IEE Proc. Microwaves, Antennas and Propagation*, Vol.145, No.3, pp263–267, June 1998.

The change in reflection coefficient (amplitude and phase) is therefore measured as a function of wire position, and the square root taken, giving a quantity directly proportional to the aperture field. The Fourier Transform of the aperture field yields the far-field radiation pattern directly. The theory is only rigorously valid for antennas whose aperture field (and hence radiation pattern) is separable - that is, expressible as the product of an x-variation and a y-variation, but this is true for many practical types of antenna. Fig. 15.12 shows a comparison of the radiation pattern of a 2 × 2 array of open-ended waveguides measured by this technique, and on a conventional far-field range.

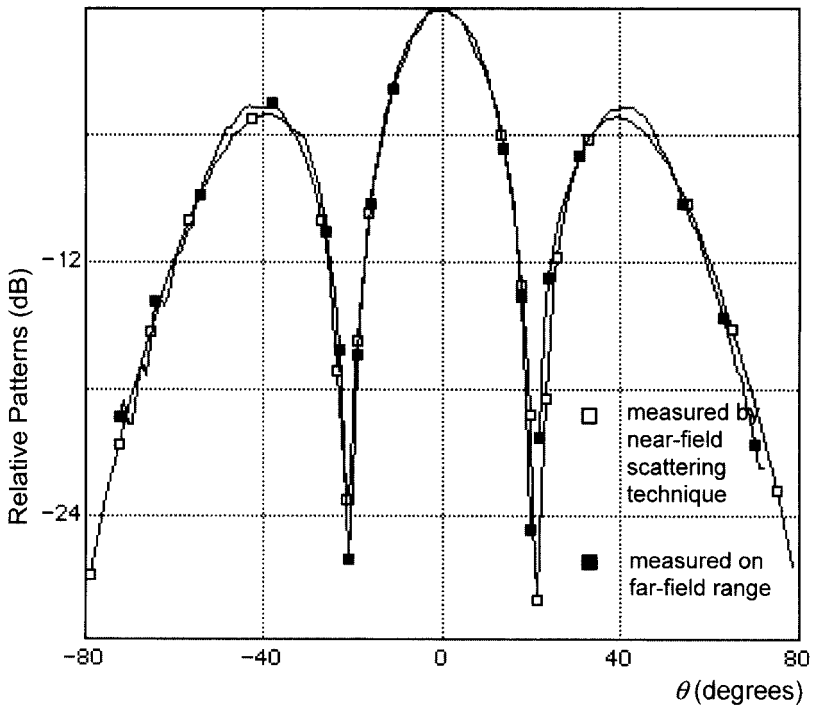

Fig. 15.12 Comparison of radiation patterns of open-ended waveguide array, computed using the wire-scattering technique (clear squares) and measured on a conventional far-field range (dark squares).

As a final comment, there are some very simple techniques that can be used with scanning radar antennas. If a probe antenna is used in the far-field, connected to a spectrum analyser in 'zero-scan' mode, tuned to the radar carrier frequency (and with IF bandwidth matched to the radar pulse length), then the time-domain sweep on the spectrum analyser screen will trace out the antenna radiation pattern (cf

Figure 13.6). The sweep speed should be adjusted to correspond to the antenna rotation rate.

15.3.6 Polarization

The polarization properties of an antenna may be measured by rotation of the source antenna. For a linearly polarized antenna, it is the co-polar and cross-polar patterns that are of interest, and these may be obtained by measuring the pattern with the source antenna aligned with the intended polarization of the antenna under test, and then repeating the measurement with the orthogonal source antenna polarization. With an elliptically-polarized antenna, the axial ratio can be measured by rotating the source antenna at a rapid rate compared with the rotation rate of the turntable. This modulates the pattern, and the peak-to-peak value of the modulation determines the axial ratio of the antenna. A pattern produced in this manner is shown in Fig. 15.13.

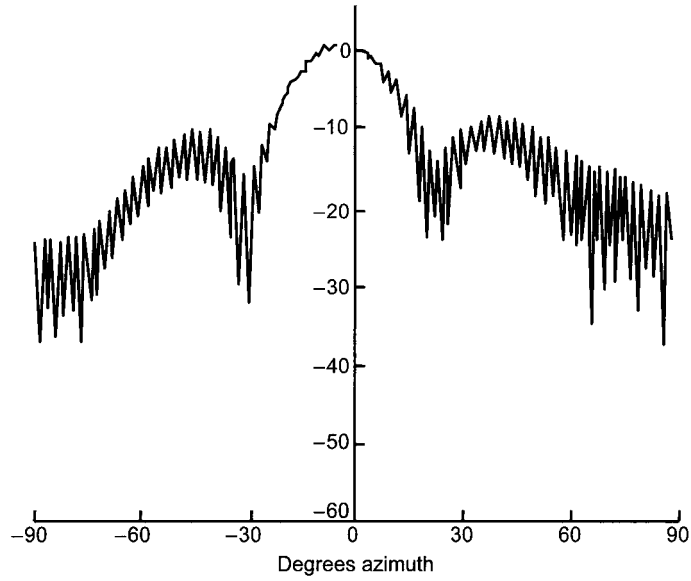

Fig. 15.13 Measurement of an elliptically-polarized antenna using a rotating linearly-polarized feed antenna. The peak-to-peak value of the modulation shows the axial ratio of the antenna under test (courtesy of Dr P. Brennan).

It should be remembered that, when measuring the gain of a circularly-polarized antenna using a linearly-polarized source antenna, the 3 dB polarization loss has to be taken into account.

15.4 TIME-DOMAIN GATING

15.4.1 Principles

A technique developed in recent years is to measure the antenna pattern with the equivalent of a short pulse, so that unwanted reflections from the chamber walls, floor and ceiling can easily be distinguished and 'gated out', thereby removing their effect[10]. In practice the time-domain response is obtained by making measurements sequentially at several frequencies and then Fourier transforming from the frequency domain into the time domain. The gating operation is then performed, and the gated signal transformed back into the frequency domain, giving 'cleaned-up' versions of the responses at the original frequencies (Fig. 15.14). The computation is made easy by routines such as those available on the Agilent HP8510 network analyser.

Denoting the measurements of transmission coefficient at a set of regularly-spaced frequencies $f_0, f_1, \ldots f_{N-1}$ by $a_0, a_1, \ldots a_{N-1}$, the samples A_k of the time-domain response are obtained by Discrete Fourier Transform of the samples a_n

$$A_k = \frac{1}{N}\sum_{n=0}^{N-1} a_n \exp\left[j(2\pi/N)nk\right] \tag{15.11}$$

The resolution in the time domain is approximately equal to the reciprocal of the total bandwidth over which the measurements are made. The wanted response can then be gated out, using a suitably-shaped window function $W(k)$, and then the inverse DFT computed

$$a'_n = \frac{1}{N}\sum_{n=0}^{N-1} A_k W(k) \exp\left[-j(2\pi/N)nk\right] \tag{15.12}$$

---

[10] Chaloupka, H., Galka, M. and Schlendermann, A., 'Determination of antenna radiation pattern from frequency-domain measurements in reflecting environment', *Electronics Letters*, Vol. 15, No. 17, pp512-513, August 1979.

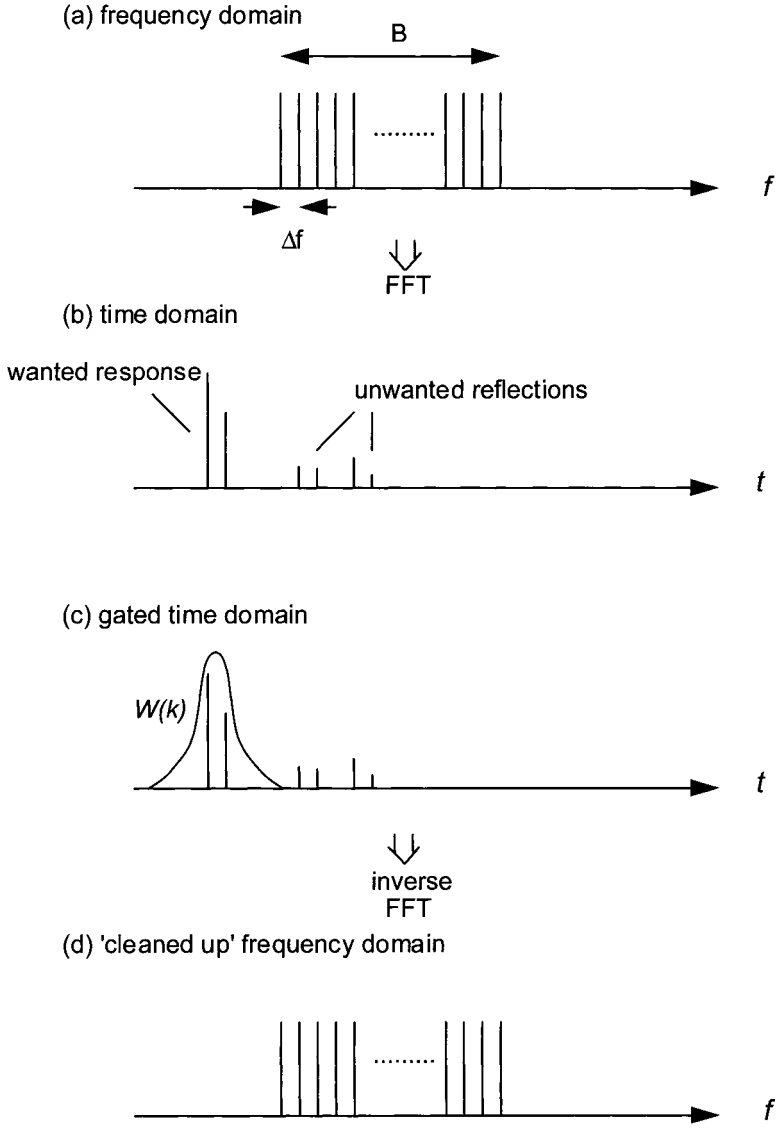

Fig. 15.14 Principle of time-domain gating.

15.4.2 Limitations

The technique has to be used with a certain amount of care. Because it makes use of measurements at other frequencies to 'clean up' the response at a single frequency, it should be used with caution with antennas whose properties are a strong function of frequency over the band implied by the range resolution. On the other hand, if the antenna is actually to be used over an instantaneously-wide band of frequencies (such as a radar using a short pulse), then arguably it is the frequency-smoothed radiation pattern that is relevant. The effect can be thought of in two (equivalent) ways. Firstly, a radiation pattern will, in general, be a function of frequency so that as the frequency is increased the main beam narrows and the sidelobe structure 'telescopes' inward. The radiation pattern measured using time-domain gating is thus an average of the patterns over a bandwidth of $1/\Delta t$, where Δt is the gate width. The averaging effect will be greatest at angles close to ±90°, tending to 'smear out' the sidelobe structure (Fig. 15.15a). Alternatively, the measurement can be considered as being made by a short pulse. Once the projected aperture of the antenna is less than the spatial extent of the pulse, then the pulse cannot excite the whole antenna simultaneously, and the sidelobe structure 'smears out' (Fig. 15.15b). Again, this effect will be greatest at angles close to ±90°.

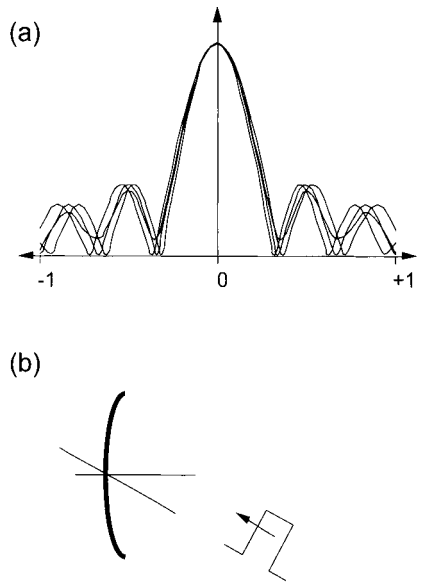

Fig. 15.15 Time-domain gating is equivalent to measurement of antenna radiation patterns over a bandwidth of $1/\Delta t$: (a) the effective pattern is an average over the bandwidth; (b) the effect can also be considered in terms of a short pulse incident at an off-boresight angle.

15.5 ANTENNA NOISE TEMPERATURE AND *G/T*

15.5.1 Measurement of antenna noise temperature

The noise temperature T_A of an antenna was defined in §4.3 as the average, weighted by the gain, of the temperatures surrounding the antenna

$$T_A = \frac{1}{4\pi} \int_{(4\pi)} T(\mathbf{u})\, G(\mathbf{u}) d\Omega \tag{15.13}$$

Clearly this depends both on the orientation of the antenna and the environment in which it is placed. For this reason, a measurement of antenna temperature must be carried out *in situ*. In principle, if the radiation pattern $G(\mathbf{u})$ is accurately known, and the function $T(\mathbf{u})$ is known or can accurately be approximated (for example, 290 K below the horizon and an appropriate value of sky temperature, according to the frequency, above the horizon), then the integration of equation (15.13) can be performed and T_A determined.

Alternatively, if the receiver noise temperature T_R is known (which will usually be the case), the receiver noise output with the antenna connected can be compared with that when a 50 Ω load (at 290 K) is connected to the receiver input. Denoting this ratio by Y

$$Y = \frac{k(T_A + T_R)B}{k(290 + T_R)B} \tag{15.14}$$

where k is Boltzmann's constant and B is the receiver noise bandwidth.

From this

$$T_A = 290Y + T_R(Y - 1) \tag{15.15}$$

15.5.2 Direct measurement of *G/T* using solar noise

Probably the simplest way of deriving G/T is to make separate measurements of G and T and to combine them. There is, however, an elegant way of measuring the ratio of gain to system noise temperature directly, using the Sun as a noise source.

Suppose firstly that the antenna is pointed at 'cold' sky. The receiver noise power, referred to the antenna terminal, is given by

$$P_n = kT_{sys}B \tag{15.16}$$

T_{sys} is the system noise temperature, and includes sky noise, ground noise via the antenna sidelobes and backlobes, and loss prior to the LNA (both as a loss and as a source of noise itself), the LNA noise temperature, and the noise temperature of any subsequent stages, weighted in each case by the inverse of the gain preceding them. P_n is therefore the noise power against which any signal must compete for detection.

Suppose now that the antenna is pointed at the Sun. The receiver noise power, referred to the antenna terminal, is now

$$P'_n = \frac{G\lambda^2}{4\pi}.\Phi B + kT_{sys}B \tag{15.17}$$

where G is the antenna gain at boresight and Φ is the solar flux, in $\mathrm{W/m^2/Hz}$.

The ratio of these noise powers may be measured (both subject to the same receiver gain), giving

$$\frac{P'_n}{P_n} = \frac{G\lambda^2\Phi B/4\pi + kT_{sys}B}{kT_{sys}B} = \frac{G\lambda^2\Phi B/4\pi}{kT_{sys}B} + 1 \tag{15.18}$$

from which the G/T ratio is given directly by

$$\boxed{\frac{G}{T_{sys}} = \frac{4\pi k}{\lambda^2\Phi}\left[\frac{P'_n}{P_n} - 1\right]} \tag{15.19}$$

The solar flux Φ is not actually constant, and three components can be distinguished: (i) a constant component (the so-called 'quiet Sun'); (ii) a slowly-varying component, varying on timescales of the order of a week; and (iii) sporadic radioemission (bursts), which last from a few seconds to a few minutes. Φ is expressed in 'solar flux units', where one solar flux unit is equivalent to $10^{-22}\ \mathrm{W/m^2/Hz}$, and values range from below 50 to over 300, a total variability of the order of 8 dB. It is also a fairly strong function of frequency, though an interpolation formula has been derived[11]:

[11] Harris, J.M., 'Measurement of phased array gain-to-temperature ratio using the solar method', Proc. *XI Antenna Measurement Techniques Association Symposium*, Monterey, pp4.26-4.31, 9-13 October 1989.

$$\Phi = \Phi_2 + (\Phi_2 - \Phi_1)\left[\left(\frac{\frac{\sqrt{f}}{f_2} - 1}{1 - \frac{\sqrt{f_1}}{f_2}}\right)\right] \tag{15.20}$$

where Φ is the desired solar flux density at frequency f, and Φ_1 and Φ_2 are the solar flux densities at frequencies f_1 and f_2 respectively.

Measurements of Φ are made at a frequency of 2.8 GHz each day at approximately 1700 UT by the Penticton Radio Observatory, British Columbia, Canada, and the results are available from various sources[12].

The solar flux will be subject to any atmospheric attenuation due to water vapour and precipitation, which under extreme conditions might be as much as 10 dB at microwave frequencies. Obviously it is best to perform the measurement on a clear, dry day when such attenuation can be ignored.

With most types of antenna likely to be measured by this method, the angular extent of the Sun (~ 0.5°) will be significant compared with the antenna beamwidth, so the solar flux is not received with equal gain across the whole of the antenna beam. The value used for the solar flux must be corrected to account for this, and the correction factor is given by

$$L_b = \frac{1}{1 - 0.163\left[\left(\frac{\phi_s}{\phi_a}\right)^2 + \left(\frac{\theta_s}{\theta_a}\right)^2\right]} \tag{15.21}$$

where $\phi_s = \theta_s$ = angular extent of the Sun, and ϕ_a and θ_a are the –3 dB azimuth and elevation beamwidths (respectively) of the antenna under consideration.

It is also possible to use this technique with 'radio stars', such as Cassiopeia-A or Cygnus-A. These are much weaker but more constant, and are a good approximation to a point source. An accuracy of ±0.3 dB has been claimed for a measurement using Cassiopeia-A of the G/T_{sys} of a 10-metre earth station.

15.6 IMPEDANCE AND BANDWIDTH

A vector network analyser may be used to measure the complex reflection coefficient ρ at the antenna feed, from which the complex antenna impedance may be derived. The antenna must be measured in a situation that is representative of its

[12] See, for example, http://www.drao.nrc.ca/icarus

operational use for this, as with any other measurement, since any structure close to the antenna could modify its impedance. In many cases only the magnitude of the mismatch is of interest, in which case the return loss, $1/|\rho|^2$, is measured. The voltage standing wave ratio (*VSWR*) and the reflection coefficient are related by

$$VSWR = \frac{1+|\rho|}{1-|\rho|} \tag{15.22}$$

from which the return loss is given by

$$\frac{1}{|\rho|^2} = \left(\frac{VSWR+1}{VSWR-1}\right)^2 \tag{15.23}$$

The transmission coefficient is $|\tau|^2 = 1-|\rho|^2$, so that the VSWR loss is

$$\boxed{|\tau|^2 = \frac{4\ VSWR}{(VSWR+1)^2}} \tag{15.24}$$

The variation of return loss and VSWR loss as a function of VSWR is shown in Table 15.1. Evidently, a high value of return loss is desirable for good matching and low VSWR loss. A device might be considered to be well matched if it has a VSWR of 2 or less, corresponding to a return loss of at least 9.5 dB and a VSWR loss of no more than 0.51 dB.

VSWR	$\|\rho\|^2$	$\|\tau\|^2$	*Return loss* (dB)	*VSWR loss* (dB)
1	0	1	∞	0
1.5	0.04	0.96	14	0.18
2	0.11	0.89	9.5	0.51
3	0.25	0.75	6	1.25
5	0.44	0.56	3.5	2.6

Table 15.1 Return loss and VSWR loss as a function of VSWR.

The bandwidth of an antenna is often limited by its input impedance. The 3 dB points are the frequencies for which the return loss (and VSWR loss) are 3 dB, corresponding to a VSWR of 5.83.

15.7 MEASUREMENTS OF CELLULAR RADIO HANDSET ANTENNAS

In recent years it has become important to be able to make reliable measurements of the radiation from mobile phone handset antennas, both to quantify the effect of any potential radiation hazard to the user, and to measure the directional properties. The radiation is significantly affected by the presence of the user's head – indeed, in some present models, more than half the radiated power may be absorbed in the user's head. This is most usually taken into account by using a 'phantom', which is a physical model of the human head with equivalent dielectric properties. Fig. 15.16 shows a typical phantom of this kind, which is filled with liquid.

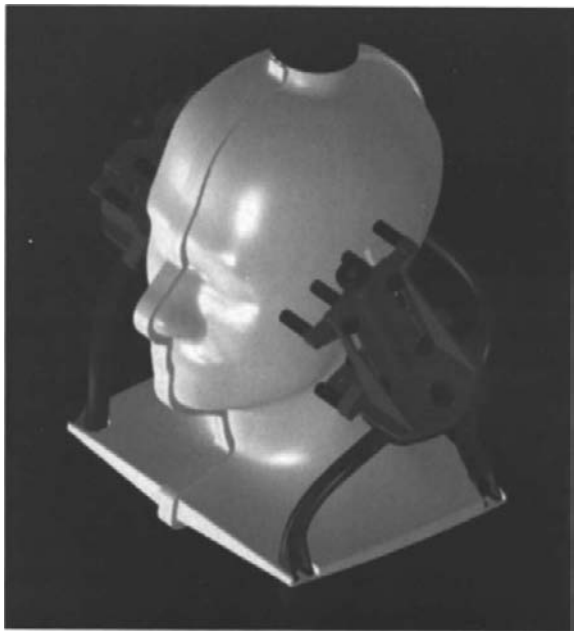

Fig. 15.16 A phantom used for measurements of handset antennas. (photograph: Schmidt and Partner Engineering AG).

15.7.1 Specific Absorption Rate

The power absorbed in materials exposed to radiation is expressed in Watts per kilogram by means of the specific absorption rate (SAR), defined as follows:

$$\text{SAR} = \frac{dP_{dep}}{dm} = \frac{\sigma |E|^2}{2\rho} \tag{15.25}$$

where ρ (kg/m^3) is the tissue density, σ (S/m) is the tissue conductivity and E is the electric field within the tissue. The recommended safe SAR values are internationally agreed and depend on a variety of factors[13] relating to how the phone is used; as a guide, a SAR of about 4 W/kg produces a temperature rise of approximately 1°C in human tissue. For mobile phones the European standard is a maximum of 2 W/kg averaged over 10g of tissue, while in the USA the value is 1.6 W/kg averaged over 1g of tissue.

Fig. 15.17 The DASY equipment (photograph: Schmidt and Partner Engineering AG).

[13] Fujimoto, K. and James, J.R., *Mobile Antenna Systems Handbook*, Artech House, 2nd edition, pp334-360, 2001.

Extensive simulation work has been carried out globally using anatomical head models to investigate SAR together with the power level contours in the brain, but most confidence is placed in field probe measurements within a tissue phantom using an actual handset. One such instrument for SAR measurement is the DASY (Dosimetric Assessment SYstem) equipment[14], manufactured by Schmidt and Partner Engineering AG in Switzerland, and shown in Fig. 15.17. This uses a probe to measure the electric field within the phantom, and hence with a knowledge of the dielectric properties the SAR can be computed from eqn. (15.25).

15.7.2 Reverberation chambers

The problem of measurement of handsets in a realistic propagation environment is also difficult. In contrast to an anechoic chamber, the requirement is to set up a realistic fading environment (see §14.7.11) in respect of the fading statistics both in amplitude and polarization.

For measurement purposes the wave polarization can be resolved into vertical polarization and horizontal polarization so in moving the mobile handset along a typical urban route the mean powers P_v and P_h respectively associated with the two polarized components can be measured. The handset antenna will not be able to capture all the polarized power and $P_r < (P_v + P_h)$, where P_r is the mean handset power that would have been received over the same route, in the same time period. The antenna performance is defined[15] in terms of its Mean Effective Gain (MEG):

$$\begin{aligned} \text{MEG} &= \frac{P_r}{(P_v + P_h)} \\ &= \int_0^{2\pi}\int_0^{\pi}\left[\frac{P_v}{(P_v+P_h)}G_\theta(\theta,\phi)P_\theta(\theta,\phi) + \frac{P_h}{(P_v+P_h)}G_\phi(\theta,\phi)P_\phi(\theta,\phi)\right]\sin\theta d\theta d\phi \end{aligned} \tag{15.26}$$

where (θ,ϕ) are spherical angular coordinates, $G_\theta(\theta,\phi)$ and $G_\phi(\theta,\phi)$ are the θ and ϕ components of the power patterns respectively, and $P_\theta(\theta,\phi)$ and $P_\phi(\theta,\phi)$ are the θ and ϕ components of the angular density functions of the incoming plane waves, respectively.

The MEG measurement process has proved useful for designing mobile antennas that give optimized performance in realistic propagation scenarios. However, the recent trend towards extreme handset compactness and internal integrated antennas (see §6.5) gives little scope for optimizing the antenna in isolation from the handset

---

[14] http://www.dasy4.com

[15] Fujimoto, K. and James, J.R., *Mobile Antenna Systems Handbook*, Artech House, 2nd edition, pp63-68, 2001.

itself. The use of reverberation chambers to test antennas in a Rayleigh fading environment is well established, but its recent application to mobile handset testing appears to offer manufacturers an efficient, low-cost method of assessing handset performance. The reverberation chamber consists of a large metal-walled cavity capable of supporting many modes which are perturbed by rotating reflectors within the excited chamber. The mode stirring is sufficiently random to create a Rayleigh distributed fading characteristic between the transmit and receive antennas within the chamber.

A demonstration chamber of this kind has recently been described[16], which has many attractive features. For example, a phantom tissue head model can be placed in close proximity to the handset under test to enable the real operating conditions to be accurately reproduced. The chamber can also be used to test the diversity functions and MIMO systems (§14.7.11). The installation costs and operating times are low, and compatible with handset manufacturing requirements.

[16] Kildal, P.S., 'Characterisation of small antennas and active mobile terminals in Rayleigh fading using reverberation chamber', *Proc. Loughborough Antennas and Propagation Conference*, pp234-239, April 2005.